analytical chemistry

Article

Surface-transfer mass spectrometry imaging of renal tissue on gold nano-particle enhanced target

Joanna Nizio#, Krzysztof Ossoli#ski, Tadeusz Ossoli#ski, Anna Ossoli#ska, Vincent Bonifay, Justyna Seku#a, Zygmunt Dobrowolski, Jan Sunner, Iwona B. Beech, and Tomasz Ruman

Anal. Chem., **Just Accepted Manuscript** • Publication Date (Web): 22 Jun 2016

ACS Publications

Analytical Chemistry is published by the American Chemical Society. 1155 Sixteenth Street N.W., Washington, DC 20036

Surface-transfer mass spectrometry imaging of renal tissue on gold nano-particle enhanced target

Joanna Nizioł,[1] Krzysztof Ossoliński,[2] Tadeusz Ossoliński,[2] Anna Ossolińska,[2] Vincent Bonifay,[3] Justyna Sekuła,[1] Zygmunt Dobrowolski,[2] Jan Sunner,[3] Iwona Beech,[3] and Tomasz Ruman[1]*

[1]*Faculty of Chemistry, Rzeszów University of Technology, Rzeszów, Poland.*

[2]*Department of General and Oncological Urology, Rzeszow City Hospital, Rzeszow, Poland,*

[3]*Department of Microbiology and Plant Biology, The University of Oklahoma, Norman, OK, USA.*

Contact data for corresponding author: Prof. Tomasz Ruman, Ph.D., D.Sc., Rzeszow University of Technology, ul. Wincentego Pola 2, 35-959 Rzeszow, Poland, Tel.: +48 17 865 1896, tomruman@prz.edu.pl

ABSTRACT

Renal cell carcinoma (RCC) accounts for several percent of all adult malignant tumor cases and is directly associated with over one hundred thousand death cases worldwide annually. Therefore, there is a need for cancer biomarker tests and methods capable of discriminating between normal and malignant tissue. It is demonstrated that gold nanoparticle enhanced target (AuNPET), a nanoparticle-based, surface-assisted laser desorption/ionization (SALDI)-type mass spectrometric method for analysis and imaging can differentiate between normal and cancerous renal tissue. Diglyceride DG(18:1/20:0) sodium adduct and protonated octadecanamide ions were found to have greatly elevated intensities in cancerous part of analyzed tissue specimen. Compounds responsible for mentioned ions formation were pointed out as a potential clear cell RCC biomarkers. Their biological properties and localization on the tissue surface are also discussed. Potential application of presented results may also facilitate clinical decision making during surgery for large renal masses.

Keywords: low molecular weight compounds; MALDI; mass spectrometry imaging; nanoparticles; renal cancer; SALDI.

INTRODUCTION

Renal cell carcinoma (RCC) accounts for 2-3% of all adult malignant tumors. RCC is an adverse malignancy, accounting for more than 80% of kidney neoplasms.[1,2] It is usually divided into three main categories, such as clear cell (ccRCC), chromophobe and papillary RCC. Relative 5-year survival for kidney cancer is 71%. According to GLOBOCAN in 2012 there were approximately 337,800 new cases of RCC and 143,400 kidney cancer-related deaths worldwide.[3]

Patients with ccRCC have the worst prognoses when compared to chromophobe or papillary subtype of RCC. Clear cell RCC has characteristic yellowish appearance, and in most cases is well circumscribed. On microscopic examination it has abundant clear cytoplasm due to high content of lipids and glycogen.[4] Tumor necrosis in analyzed sample pathological report represents unfavorable features and is significantly associated with higher risk of death from ccRCC.[5]

As there are several different types of RCCs with different survival rates, specific biomarkers are needed for early detection and monitoring of recurrence and response to treatment.[6,7] Since the introduction of mass spectrometric techniques for proteomics, numerous attempts have been made to discover cancer-specific proteins and peptides.[8] It was shown that it is possible to employ matrix-assisted laser desorption ionization/mass spectrometry (MALDI MS) for identification of biomarkers for bladder cancer in urine.[9,10] Similarly, alterations of peptide level in serum were used to distinguish benign and malignant tumors of RCC.[11]

With the development of MALDI/MS for imaging of proteins, it became possible to combine conventional proteomic techniques for protein identification with mass spectrometric imaging for the correlation with spatial information.[12-15] Conventional MALDI imaging requires that tissue sections are placed on a conductive surface, such as that of a metal or of indium tin oxide (ITO)-coated glass followed by the careful application of a suitable matrix on the sample surface.

Herring et al. reported the application of MALDI imaging to cancer-invaded kidney tissue for the correlation of protein distributions with local disease states.[16] MALDI imaging has further been successfully applied to the identification of peptides present in clear cell RCC (ccRCC) through the detection of peptide signatures from *in-situ* trypsin-treated tissues by Morgan et al.[17] Identified peptides that were derived from proteins, such as vimentin, α-enolase and histone 2A, may be considered as potential peptide signatures for ccRCC. Using MALDI imaging in combination with liquid chromatography MS/MS (LC-MS/MS), Kim et al. group focused on two proteins, S100A11 and the ferritin light chain, that are specific for papillary RCC cancer regions.[2]

MALDI imaging MS has been investigated as a tool to assist grading of urothelial neoplasms and to improve its accuracy.[18] The method has also recently been employed for the analysis of a microarray of renal tissue samples from 789 patients. Comparison of the mass spectrometric signals with clinico-pathological features revealed significant differences between, for example, papillary and clear cell renal cell cancer.[19]

These early results demonstrate that MALDI MSI must be considered as a powerful tool for biomarker discovery. However, well-known drawbacks of MALDI include (i) abundant and numerous chemical background peaks in the low-mass region ($m/z < \approx 1{,}000$) due to the presence and ionization of the applied matrix; (ii) the frequent need for external mass calibration; (iii) low mass resolution and accuracy due to the thickness of the tissue samples; (iv) low ionization efficiency for many organic compounds, present in the samples in their noncharged states; (v) inhomogeneous matrix crystallization; and (vi) commonly observed acid-catalyzed hydrolysis of various biomolecules. In particular, these problems make MALDI unsuitable for the identification, analysis and imaging of low-molecular-weight compounds, and thus for metabolomic biomarker research.

To circumvent these limitations, we here report on the application of the gold nanoparticle-enhanced target (AuNPET) laser desorption/ionization MS method for metabolic biomarker discovery. AuNPET,[20] which belongs to the surface-assisted laser desorption/ionization (SALDI)[21]

type of methods, circumvents many of the problems of MALDI. Results from AuNPET analysis and imaging of RCC samples, with a focus on biomarker discovery, are reported. It should be noted that there are no RCC imaging results made with the use of nanoparticle-based methods published to date.

EXPERIMENTAL SECTION

Enrollment of patients

After receiving protocol approval from the bioethics committee at the University of Rzeszow (Poland), eleven patients with kidney cancer scheduled for radical nephrectomy were enrolled in the study between March and December of 2015. Informed consent was obtained from all patients. Each patient donated 10 ml of blood, 100 ml of urine and 1 cm^3 of cancerous and normal renal tissue removed *ex vivo* after surgical resection of kidney. The specimen described in this work was obtained from an 80-year-old, asymptomatic female with diabetes type II, hypertension and hyperthyroidism. A CT (X-ray computed tomography) scan revealed the presence of a 79x89x81 mm tumor, localized in the lower pole of the right kidney and with no nodal involvement or distant metastases. All laboratory test results (complete blood count, kidney function tests, CRP, urine analysis, bleeding profile) were within normal limits. Pathological analysis confirmed the malignant character of the tumor - renal cell carcinoma (RCC), subtype: clear cell, Fuhrman III with 10% necrosis within tumor and invasion into kidney capsule.

Materials.

AuNPET targets were prepared on stainless steel plates, as previously described.[22] All solvents used in this work were of HPLC purity.

Methods

Laser desorption/ionization (LDI) MS and MS/MS analysis of tissue extracts on AuNPET

LDI MS and MS/MS experiments were performed in reflectron mode using a time-of-flight mass spectrometer (Bruker Daltonics, Autoflex™ Speed). The instrument is equipped with a pulsed, 352 nm solid-state laser (Bruker Daltonics, 1 kHz SmartBeam II) operated at a laser pulse repetition rate of 1000 Hz and with a laser pulse energy of approximately 100−190 μJ. In reflectron mode, the operating voltages were as follows: ion source 1, 19 kV; ion source 2, 16.7 kV; lens 8.4 kV; reflector 1, 21 kV; reflector 2, 9.55 kV. The pulsed ion extraction (PIE) delay time was 150 ns. Spectra were recorded in positive ion mode in the *m/z* range of 80-2000, with ions below *m/z* 80 deflected from the flight tube. All spectra were internally mass calibrated using the gold ion clusters (Au^+ to Au^{7+}) peaks observed in all mass spectra. Mass calibration employed - a best fit to a cubic equation, based on 5-10 internal mass standards (gold ions and clusters from Au^+ to Au_{10}^+). MS/MS measurements were performed using the LIFT™ (low mass) method.[23] FlexAnalysis (version 3.3, Bruker) was used for data analysis.

Sample preparation

Normal and cancer tissue samples for MS and MS/MS analyses were collected (approx. 1 mg) from central parts of both RCC and normal tissue (*ca.* 1x1 mm area of sample collection) of specimen used in imaging experiment. The samples were first ultrasonicated in water (100 μL) or tetrahydrofuran (100 μL) producing extracts for MS analyses. The extracts (0.3 μL) were separately applied to the AuNPET substrates (see below), The sample spots were air-dried and analyzed in the time-of-flight (ToF) mass spectrometer.

LDI MS Imaging

Measurements were performed using the time-of-flight mass spectrometer (Bruker Daltonics, Autoflex™ Speed) in reflectron mode. The instrument is equipped with a pulsed, 352 nm solid-state laser (Bruker Daltonics, 1 kHz SmartBeam II) operated at a laser pulse repetition rate of 1000 Hz and with a laser pulse energy of approximately 100−190 μJ. The spatial resolution in

imaging mode was 150 × 150 μm and, in each individual spot, mass spectra were recorded from 500 laser shots, using the default random walk method (Bruker, FlexImaging 4.0). Spectra were recorded in positive ion mode in the *m/z* range of 80-2000, with ions below *m/z* 80 deflected from the proper ion trajectory. In reflectron mode, the operating conditions voltages were as follows: ion source 1, 19 kV; ion source 2, 16.7 kV; lens 8.4 kV; Reflector 1, 21 kV; reflector 2, 9.55 kV. The delay time was 150 ns. All spectra were externally mass calibrated using gold ion clusters (Au^+ to Au^{7+}). All images shown were constructed using an *m/z* window of ± 0.01%, and TIC normalization was used throughout.

Tissue sample for MS imaging was used as received after surgery. The tissue surface selected for imaging has a dry appearance with no shiny, visible liquid on its surface. Material was transferred to the AuNPET target surface by allowing the two surfaces to touch each other for one second followed by sample removal and drying of target with flow of nitrogen. Peaks obtained in MS experiments were identified with the aid of Human Metabolome Database[24] and LIPID Metabolites and Pathways Strategy.[25] Experimental and calculated isotopic distributions were compared for all of ions listed in Table 1. Calculated/experimental *m/z* differences for all identified compounds are below 5 ppm. Other identification methods were also used as mentioned in Results and Discussion.

RESULTS AND DISCUSSION

AuNPET imaging of RCC specimen

In order to test the applicability of AuNPET/MS to the analysis of human tissue, in general, and to cancer biomarker discovery, in particular, several series of analyses were conducted. The chosen object was surgically removed clear cell subtype of renal cell carcinoma with visible borders between cancerous tissue (RCC), perinephric fat and normal kidney tissue with distinguishable renal papilla, all separated by tumor pseudocapsule (Figure 1A). Material was transferred from the

RCC object to the AuNPET substrate by briefly touching the two surfaces, as described in Methods (Section 2.3). After drying with a flow of nitrogen gas for 2 minutes, the target was inserted into MS ion source. The process is very rapid; the total time required from receiving of cancer tissue until the target has been inserted into the ion source was 3-4 minutes.

Material transferred from the object to the AuNPET surface was easily observed by visual examination or by optical low-magnification microscopy, allowing the appropriate area coordinates for the imaging to be specified in the software. Additionally, a 'chemical photograph' of transferred material (Figure 1B) was constructed by superposing the ion images of *m/z* 207.1, 184.1 and 907.7, each containing information about different regions of the analyzed specimen. This kind of image was previously shown to be very helpful, both in determining the location of total material transferred to the AuNPET plate and in locating key-structural elements of the imaged object.[20] The size of the imaged area of the RCC sample was *ca.* 25x15 mm. The spatial resolution was 150x150 micrometer; mass spectra were obtained for 18719 pixels; and the time required to obtain the image was approximately 12 hours.

The MS imaging data contains not only spatial information, but also information on what compounds are present in the sample. Comparison of list of peaks with HMDB database allowed to prepare list of peaks of interest which were additionally visually correlated with specimen structure. Interesting ions and their ion are shown in Table 1. It should be noted that all ions shown in Table 1 were found in both water and THF extracts.

One of the most interesting compounds found in LDI MS spectrum analysis was glutamine, considered to be a potential RCC biomarker.[26] MS imaging proved that considering protonated ion intensities, this compound was found in external parts of both normal and cancer tissue regions (Figure 1 K).

Table 1. Tentative identification[24] of selected mass peaks observed in the RCC MS imaging

Compound name	Ion formula	$m/z_{calc.}$[1]	*Image*
Glutamine[2]	$[C_5H_{10}N_2O_3 + H]^+$	147.0764	Fig. 1K
2-Propionyl-2-thiazoline[2]	$[C_6H_9NOS + Na]^+$	166.0297	Fig. 1F
Glutamic acid[2]	$[C_5H_9NO_4 + K]^+$	186.0163	Fig. 1D
Dihydrowyerone[2]	$[C_{15}H_{16}O_4 + Na]^+$	283.0941	Fig. 1E
Octadecanamide	$[C_{18}H_{37}NO+H]^+$	284.2948	Fig. 1I
Eicosenoic acid[2]	$[C_{20}H_{38}O_2+H]^+$	311.2945	Fig. 1C
3-(8,11,14-Pentadecatrienyl)phenol[2]	$[C_{21}H_{30}O + K]^+$	337.1928	Fig. 1J
Sodium oleate[2]	$[C_{18}H_{33}O_2Na + K]^+$	343.2010	Fig. 1G
2-Methyl-5α-androst-2-en-17β-ol acetate	$[C_{22}H_{34}O_2 + K]^+$	369.2190	Fig. 1H
4,4'-Diaponeurosporene[2]	$[C_{27}H_{43}OF + K]^+$	441.2930	Fig. 2I
Camelliol C[2]	$[C_{30}H_{50}O + Na]^+$	449.3754	Fig. 2H
DG(15:0/18:2)[2]	$[C_{36}H_{66}O_5 + Na]^+$	603.4959	Fig. 2J
DG(14:0/20:0)[2]	$[C_{37}H_{72}O_5 + Na]^+$	619.5272	Fig. 2K
PG(P-16:0/12:0)[2]	$[C_{34}H_{67}O_9P + H]^+$	653.4752	Fig. 2O
DG(18:1/20:0)	$[C_{41}H_{78}O_5 + Na]^+$	673.5747	Fig. 2N
PG(14:1/14:1)[2]	$[C_{34}H_{63}O_{10}P + Na]^+$	685.4051	Fig. 2M
PG(13:0/15:1)[2]	$[C_{34}H_{65}O_{10}P + Na]^+$	687.4208	Fig. 2L
PG(14:1/20:5)[2]	$[C_{40}H_{67}O_{10}P + H]^+$	739.4545	Fig. 2S
Solanesyl diphosphate[2]	$[C_{45}H_{76}O_7P_2 + H]^+$	791.5139	Fig. 2R
PE(40:2)[2]	$[C_{45}H_{86}NO_8P+H]^+$	800.6164	Fig. 2Q
PS(18:3/20:5)[2]	$[C_{44}H_{70}NO_{10}P + H]^+$	804.4810	Fig. 2P
PS(P-16:0/22:6)[2]	$[C_{44}H_{74}NO_9P + Na]^+$	814.4993	Fig. 2W
PA(20:0/22:6)[2]	$[C_{45}H_{77}O_8P + K]^+$	815.4988	Fig. 2V
Vinaginsenoside R11[2]	$[C_{41}H_{70}O_{14} + K]^+$	825.4397	Fig. 2U
PS(38:7)[2]	$[C_{44}H_{72}NO_{10}P + Na]^+$	828.4786	Fig. 2T
	$[C_{44}H_{72}NO_{10}P + K]^+$	844.4525	Fig. 2G
20:1-Glc-campesterol[2]	$[C_{54}H_{94}O_7 + H]^+$	855.7072	Fig. 2F
TG(12:0/20:4/22:6)[2]	$[C_{57}H_{90}O_6 + H]^+$	871.6810	Fig. 2E
PC(O-18:1/24:0)[2]	$[C_{50}H_{100}NO_7P + Na]^+$	880.7130	Fig. 2D
TG(54:8)[2]	$[C_{57}H_{94}O_6 + Na]^+$	897.6943	Fig. 2C
PC(O-22:1/22:2)[2]	$[C_{52}H_{100}NO_7P + Na]^+$	904.7130	Fig. 2B
22:0-Glc-Campesterol[2]	$[C_{56}H_{100}O_7 + Na]^+$	907.7361	Fig. 2A

[1]Calculated *m/z* vaules; [2]putative metabolite. DG: diacylglyceride; TG: triacylglyceride; PA: phosphatidylglycerol; PC: phosphocholine; PG: glycerophosphoglycerols; PS: phosphatidylserine; PE: glycerophosphoethanolamines.

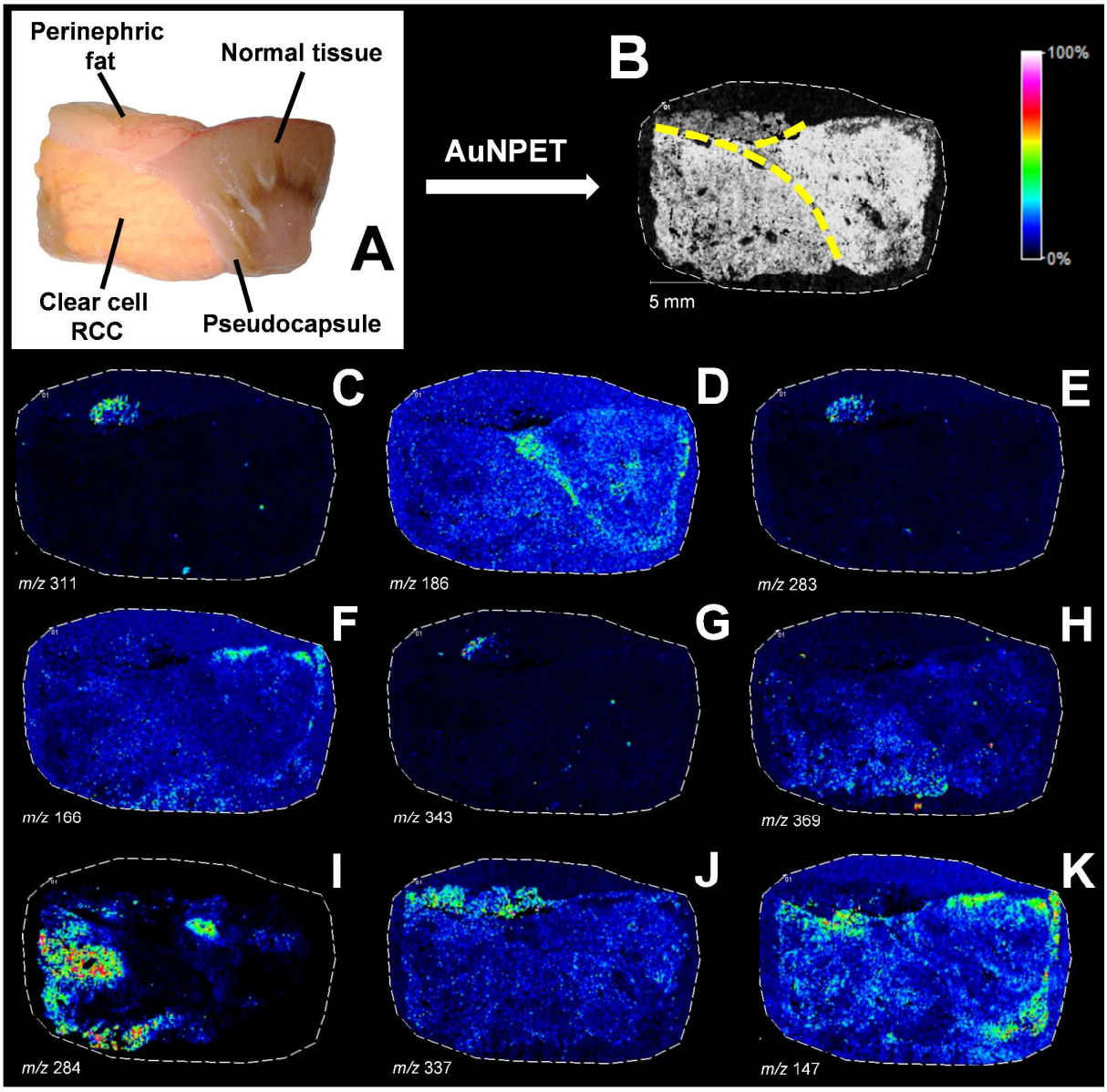

Figure 1. Optical photograph of the imaged surface of the renal cancer carcinoma (RCC) specimen (A); sum of selected ion images with total abundance in each pixel displayed on a gray scale and with the different regions delineated by the yellow dashed lines (B). Images C-K present ion images for *m/z* values of 311.29 (C), 186.02 (D), 283.09 (E), 166.03 (F), 343.20 (G), 369.22 (H), 284.29 (I), 337.19 (J) and 147.08 (K), respectively. Spatial resolution of ion images is 150 x 150 µm.

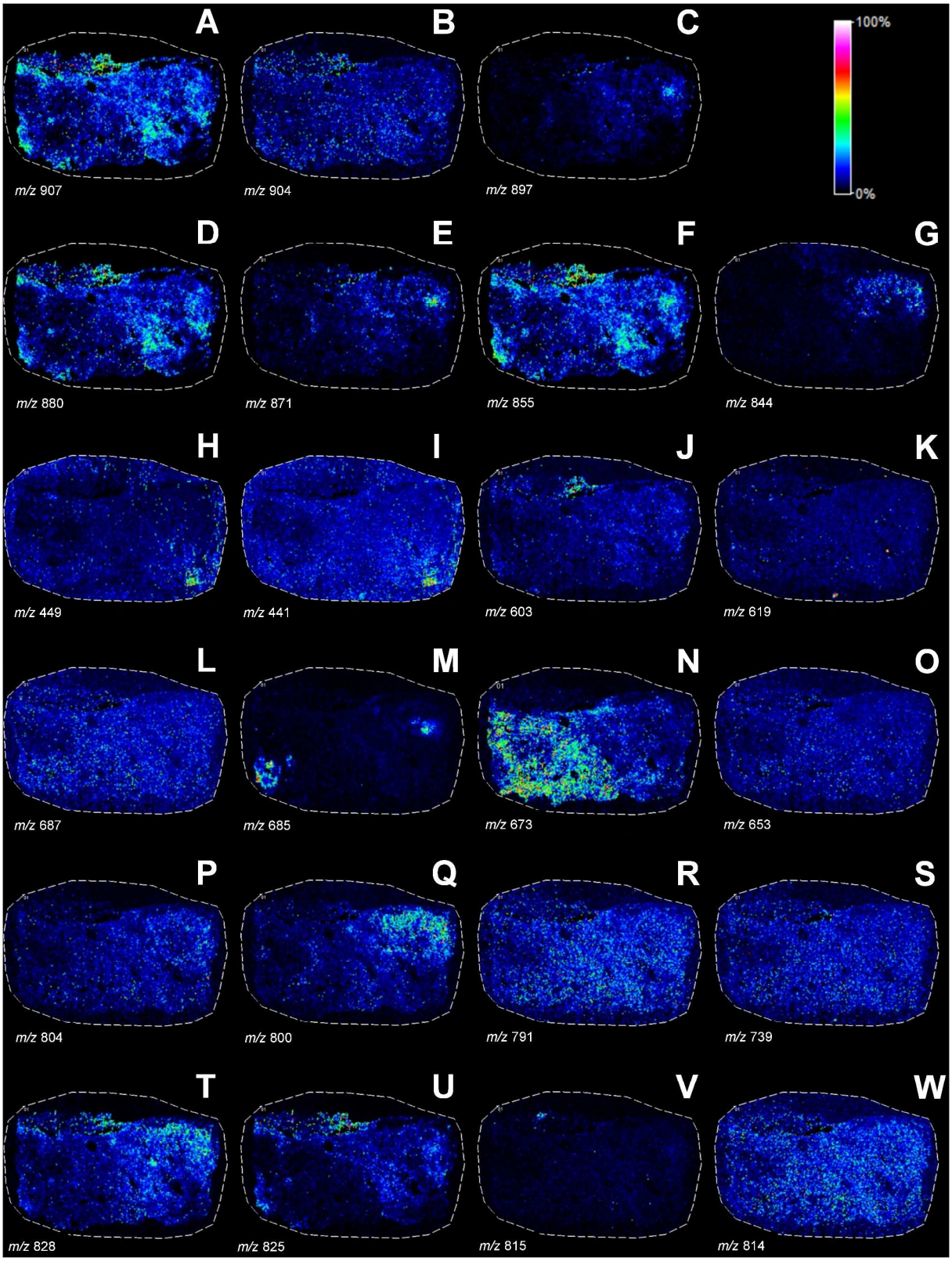

Figure 2. Ion images (A-W) of the same area of the RCC as shown in Figure 1 for *m/z* values of 907.74 (A), 904.71 (B), 897.70 (C), 880.71 (D), 871.68 (E), 855.71 (F), 844.45 (G), 449.38 (H), 441.29 (I), 603.50 (J), 619.53 (K), 687.42 (L), 685.41 (M), 673.57 (N), 653.48 (O), 804.48 (P),

800.62 (Q), 791.51 (R), 739.45 (S), 828.47 (T), 825.44 (U), 815.49 (V), 814.49 (W) respectively. Spatial resolution – 150 x 150 μm.

Inspection of the selected ion images reveals a variety of different patterns, which reflect the concentrations of the corresponding parent compounds. Of particular interest are those compounds whose abundance correlates with the different tissue region, as illustrated in Figures 1A and 1B. For example, the ions of low polarity compounds found at *m/z* 311.29, 283.09, 343.20 and 337.19 (Figure 1C,E,G,J) have the highest abundance in the perinephric fat region of analyzed specimen. Other ions, such as *m/z* 619.53, 653.48, 804.48, 791.51, 739.45 and 814.50 (Figure 2K,O,P,R,S and W, respectively) are detected at similar abundances throughput the images surface. Similarly, ion images visible in Figure 2C,G-I,Q,T,U, are having highest intensities in various parts of normal tissue. In contrast to the above mentioned distributions, images H (Figure 1) and N (Figure 2) present clearly highest ion intensities in cancer region. Compounds forming ions of *m/z* values of 369.2190 (H) and 673.5747 (N) are discussed below.

One of the most interesting single ion images can be seen in Figure 1I or Figure 3D and belongs to protonated octadecanamide ion. The confirmation of identity of this compound was aided by LIFT™ fragmentation and also comparison of isotopic distribution (Supporting Information S1). Mentioned ion was found mainly in the cancer region of analyzed specimen, but also small regions of much lower intensity of this ion were found in normal tissue. Detailed analysis of this sample suggest that its presence in normal tissue region is associated with existence of blood vessel. As can be seen in Figure 3E, spectra extracted from cancer and normal tissue regions presents very big difference in intensity for this ion being few thousands for cancer and just dozens for normal tissue regions. It should be noted that much lower intensity of protonated octadecanamide ion peak in normal tissue region cannot be explained by less probable effects such as local differences of nanoparticle activity or different thickness of transferred material as intensities of neighboring gold ions Au^+ (*m/z* approx. 197) and Au_2^+ (*m/z* approx. 394) are quite

similar in cancer (Figure 3A,C, top) and normal (Figure 3A,C, bottom) regions. This magnitude of difference of intensity of octadecanamide ion may be a very desirable feature considering detection of cancer tissue. Mentioned effect probably originate from high affinity of low-polarity compound to gold nanoparticles, an effect similar to nanoparticle-based solid phase extraction, a technique used for enrichment of low-polarity compounds.[27]

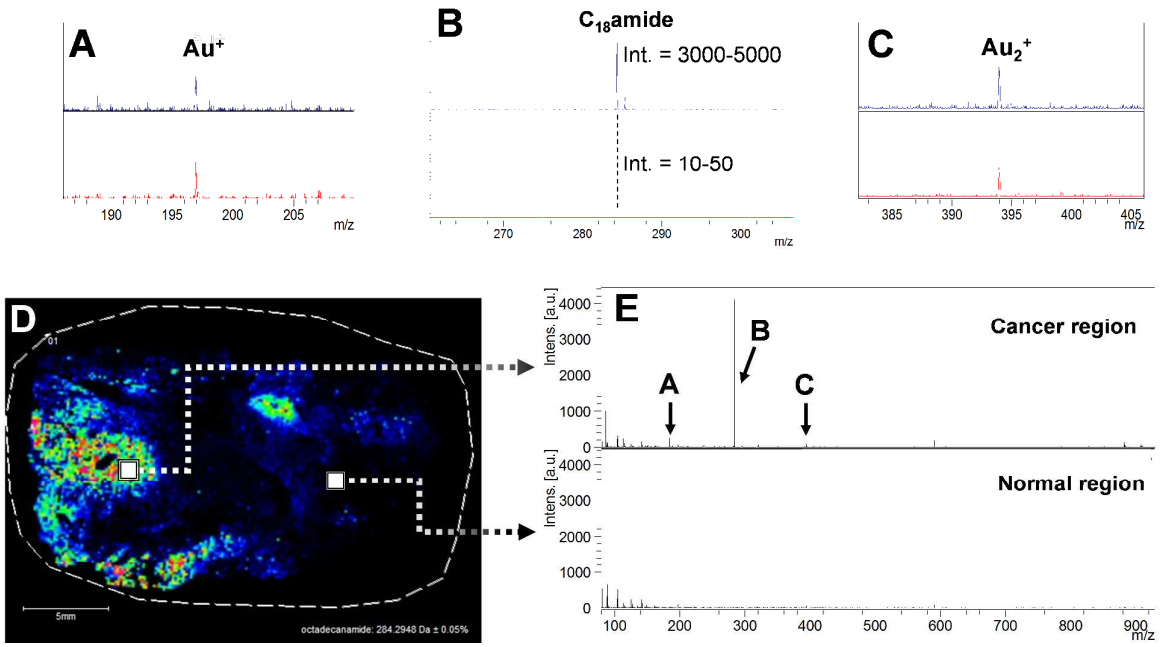

Figure 3. Ion image generated for protonated octadecanamide ion, *m/z* 284.29 (D). Parts A-C and E of figure presents extracted spectra for areas marked with white squares for both cancer (B, upper spectrum) and normal region (B, lower spectrum) of the sample.

Compound which cationisation product was found at *m/z* 369.2190 was analyzed with the use of LIFT fragmentation (Supporting Information S2) which proved that it contains one AcO group, at least two methyl groups and a steroid-type skeleton. Careful examination of potential candidates found in HMDB database suggested that only one compound fits to all of the conditions - 2-methyl-5-androst-2-en-17-ol acetate. However, also other isomers that are not listed in human metabolomic databases and containing above mentioned functional groups could also fulfill presented conditions.

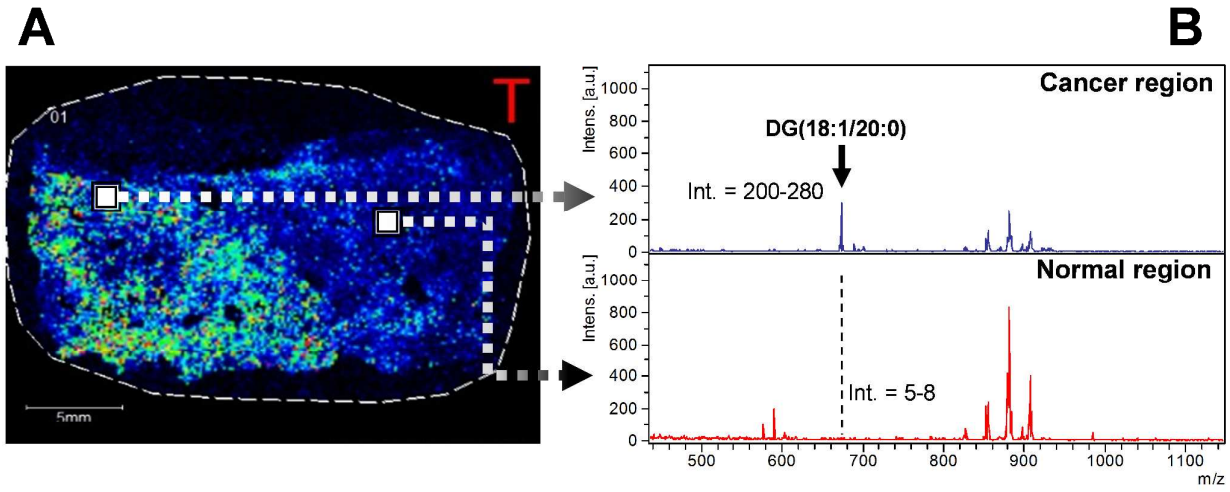

Figure 4. Ion image generated for DG(18:1/20:0)-sodium adduct, *m/z* 673.57 (A). Part B of figure presents extracted spectra for areas marked with white squares for both cancer (B, upper spectrum) and normal region (B, lower spectrum) of the sample.

One of the most interesting images obtained with the use of AuNPET LDI MS method is presented in Figure 4A. The comparison of this image with merged ion image (Figure 1B) proves that the most intense signals were found only on cancer region of the analyzed sample. Analysis of Figure 4A suggest that AuNPET-based imaging could be also considered useful for accurate distinguishing between malignant from normal renal tissue. Extracted spectra from cancer and normal regions (white squares, Figure 4 A) shown in Figure 4 B demonstrates that there is an unexpected, very high difference of intensity of *m/z* 673.57 ion peak. Mentioned peak intensity in cancer tissue was found to be in 200-280 range, while this values were much smaller for normal region being in 5-8 range of the relative intensity scale. The 25-56 higher intensity of this potential cancer biomarker is much higher than for the most of reported biomarkers.

The 673.57 peak was identified as diglyceride DG(18:1/20:0)-sodium adduct on the basis of isotopic distribution as well as LIFT fragmentation (Supporting Information S3-5). It is noteworthy that discussed compound was never mentioned in literature as a potential RCC biomarker. What is more, this compound was absent in commonly made electrospray ionization (ESI)-based analysis of

the same cancer extract. The cause of this phenomenon is most probably high affinity of discussed diglyceride to gold nanoparticles.

High concentration of DG in cancerous tissue as observed in our study may be connected with activity of phospholipase C (PLC) which is also dependent on protein kinase C. Numerous studies have shown involvement of protein kinase C (PKC) in cancerogenesis. PKC are a family of serine/threonine protein enzymes that directly controls function of other proteins by phosphorylation of hydroxyl group of serine and threonine. Mentioned enzyme also indirectly controls various cellular processes including proliferation and apoptosis. Dysregulation in the balance between those two processes contribute to cancerogenesis. Rising concentration of calcium ions (Ca^{2+}) or diacylglycerol (DG) activates PKC and promotes its relocation from the cytoplasm to the cellular membrane. DG is the end product of hydrolysis of phosphatidylinositol 4,5-bisphosphate (PIP2) by phospholipase C (PLC). Overexpression of different PKC-isomers were reported in bladder, brain, colon, breast, prostate and renal cancer. According to Brenner et al., increased expression of PKC correlates with renal cell carcinoma grading.[28] Moreover, Chuize and co-workers have shown that the higher was the PKC (isomer alpha) membrane to cytosol (M/C) ratio, the more advanced was the renal carcinoma both in grade and stage.[29] There is also growing evidence linking PLC expression to metastatic potential of the tumor by promoting neo-angiogenesis and dysregulation of integrins.[30]

From the medical point of view, current imaging methods (computer tomography, magnetic resonance imaging) nor intraoperative histological examination of resected specimen cannot differentiate between benign and malignant renal tumor. Such diagnosis pre-operatively can only be established with renal biopsy. However, it is not a standard procedure made before renal cancer surgery and it can be only employed in selected cases. It is made mainly to obtain histological results before ablative treatment, to select patients for surveillance approaches and in setting of metastatic disease to choose the most suitable targeted pharmacologic therapy. Studies have shown that up to 22% of renal biopsies are non-diagnostic.[31] Insufficient specimen volume, interobserver

inconsistency in pathologic report, complicated renal tumors histopathology, histological heterogeneity within a tumor or tumor necrosis, all constitutes diagnostic difficulties.

Because of high risk of positive surgical margins and unfavorable prognosis, European Association of Urology guidelines recommends to favor radical nephrectomy over nephron-sparing surgery (NSS)/partial nephrectomy for large renal tumors. However, after confirming non-malignant nature of the tumor, possibly with intraoperative MS examination, when risk of positive margins is not clinically significant, NSS could be technique of choice. Those patients would benefit from lesser decline of renal function after surgery and have better quality of life. Numerous studies have shown that positive surgical margins after NSS may be as high as 7% and it is associated with increased risk of local recurrence. Standard intraoperative evaluation of frozen sections yields high false negative or inconclusive results and do not correlate well with final pathological result.[32,33] A promising solution to this problem may be similar to the one shown by Eberlin who proved that mass spectrometric imaging may be a method of choice for assessing surgical margins after surgery for gastric cancer.[34] Considering clear differentiation between tumor and normal tissue shown in Figure 4A, it may be stated that methodology presented in this work may be suitable for determination of surgical margins of ccRCC.

CONCLUSIONS

Laser desorption/ionization mass spectrometry with the use of nanoparticle-enhanced SALDI-type target AuNPET was used for analysis and imaging of normal and cancer tissue regions of a single specimen removed surgically from patient. Ion images produced for few dozens of compounds of interest presented attention-grabbing differentiation of intensities. Few most important compounds were discussed in detail with attention to their biological significance. Diglyceride DG(18:1/20:0) and octadecanamide were pointed out as a potential biomarkers.

ASSOCIATED CONTENT

Supporting Information Available: This material is available free of charge via the Internet at http://

http://pubs.acs.org. Supporting information: compound identification data (S1-S5).

AUTHOR INFORMATION

Corresponding Author: tomruman@prz.edu.pl

Notes: The authors declare no competing financial interest

ACKNOWLEDGMENTS

Research was supported by National Science Center (NCN Poland; PRELUDIUM project no. UMO-2015/19/N/ST4/00379). We also thank German and Polish Bruker-Daltonics for FlexImaging 4.0.

REFERENCES

(1) Motzer, R.J.; Bander, N.H. and Nanus, D.M. *N Engl. J. Med*. **1996**, *335*, 865-875.
(2) Na, C.H.; Hong, J.H.; Kim, W.S.; Shanta, S.R.; Bang, J.Y.; Park, D.; Kim, H.K. and Kim, K.P. *Mol. Cells* **2015**, *38(7),* 624-629.
(3) Ferlay, J.; Soerjomataram, I.; Ervik, M.; Dikshit, R.; Eser, S.; Mathers, C.; Rebelo, M.; Parkin, D.M.; Forman, D.; Bray, F. GLOBOCAN 2012 v1.0, Cancer Incidence and Mortality Worldwide, IARC CancerBase No. 11 Lyon, France, International Agency for Research on Cancer; **2013**.
(4) Shuch, B.; Amin, A.; Armstrong, A.J.; Eble, J.N.; Ficarra, V.; Lopez-Beltran, A.; Martignoni, G.; Rini, B.I.; Kutikov, A. *European Urology* **2015**, *67*, 85–97.
(5) Cheville, J.C.; Lohse, C.M.; Zincke, H.; Weaver, A.L.; Blute, M.L. *Am J Surg Pathol*. **2003**, *27*, 612–24.
(6) Schwamborn, K. and Caprioli, R.M. *Nature Reviews Cancer* **2010**, 639-646.
(7) Siu, K.W.; DeSouza, L.V.; Scorilas, A.; Romaschin, A.D.; Honey, R.J.; Stewart, R.; Pace, K.; Youssef, Y.; Chow, T.F.; and Yousef, G.M. *J. Proteome Res*. **2009**, *8*, 3797-3807.
(8) Seliger, B.; Dressler, S.P.; Lichtenfels, R. and Kellner, R. *Proteomics* **2007**, *7*, 4601-4612.
(9) Li, F.; Chen, D.N.; He, C.W.; Zhou, Y.; Olkkonen, V.M.; He, N.; Chen, W.; Wan, P.; Chen, S.S.; Zhu, Y.T.; Lan, K.J.; Tan, W.L. *J. Proteomics* **2012**, *77*, 225–236.
(10) Bryan, R.T.; Wei, W.B.; Shimwell, N.J.; Collins, S.I.; Hussain, S.A.; Billingham, L.J.; Murray, P.G.; Deshmukh, N.; James, N.D.; Wallace, D.M.A.; Johnson, P.J.; Zeegers, M.P.; Cheng, K.K.; Martin, A.; Ward, D.G. *Proteom. Clin. Appl.* **2011**, *5*, 493–503.

(11) Gianazza, E.; Chinello, C.; Mainini, V.; Cazzaniga, M.; Squeo, V.; Albo, G.; Signorini, S.; Di Pierro, S.S.; Ferrero, S.; Nicolardi, S.; van der Burgt, Y.E.M.; Deelder, A.M.; Magni, F. *J. Proteomics* **2012**, *76*, 125–140.
(12) Chaurand, P.; Schwartz, S.A. and Caprioli, R.M. *Curr. Opin. Chem. Biol.* **2002**, *6*, 676-681.
(13) Chaurand, P.; Schwartz, S.A.; Reyzer, M.L. and Caprioli, R.M. *Toxicol. Pathol.* **2005**, *33*, 92-101.
(14) Francese, S.; Dani, F.R.; Traldi, P.; Mastrobuoni, G.; Pieraccini, G. and Moneti, G. *Comb. Chem. High Throughput Screen* **2009**, *12*, 156-174.
(15) Stoeckli, M.; Chaurand, P.; Hallahan, D.E. and Caprioli, R.M. *Nat. Med.* **2001**, *7*, 493-496.
(16) Herring, K.D.; Oppenheimer, S.R.; Caprioli, R.M.; *Semin. Nephrol*. **2007**, *27*, 597–608.
(17) Morgan, T.M.; Seeley, E.H.; Fadare, O.; Caprioli, R.M. and Clark, P.E. *J. Urol*. **2013**, *189*, 1097-1103.
(18) Oezdemir, R.F.; Gaisa, N.T.; Lindemann-Docter, K.; Gostek, S.; Weiskirchen, R.; Ahrens, M.; Schwamborn, K.; Stephan, C.; Pfister, D.; Heidenreich, A.; Knuechel, R.; Henkel, C. *Clin. Biochem.* **2012**, *45*, 7–11.
(19) Steurer, S.; Seddiqi, A.S.; Singer, J.M.; Bahar, A.S.; Eichelberg, C.; Rink, M.; Dahlem, R.; Huland, H.; Sauter, G.; Simon, R.; Minner, S.; Burandt, E.; Stahl, P.R.; Schlomm, T.; Wurlitzer, M.; Schlüter, H. *Anticancer Res.* **2014**, *34(5),* 2255-61.
(20) Sekuła, J.; Nizioł, J.; Misiorek, M.; Dec, P.; Wrona, A.; Arendowski, A. and Ruman, T. *Analytica Chimica Acta*, **2015**, *895*, 45-53.
(21) Sunner, J.; Dratz, E.; Chen, Y-C. *Analytical Chemistry* **1995**, *67*, 4335–4342.
(22) Sekuła, J.; Nizioł, J.; Rode, W. and Ruman, T. *Analytica Chimica Acta* 2015; *875*, 61–72.
(23) Suckau, D.; Resemann, A.; Schuerenberg, M.; Hufnagel, P.; Franzen, J.; Holle, A. *Anal Bioanal Chem* **2003**, *376*, 952–965.
(24) Wishart, D.S.; Jewison, T.; Guo, A.C.; Wilson, M.; Knox, C.; et al.; *Nucleic Acids Res*. **2013**, *41(D1),* D801-7.23161693
(25) Fahy, E.; Sud, M.; Cotter, D. and Subramaniam, S. *Nucleic Acids Research* **2007**, *35*, W606-12.
(26) Gaoa, H.; Dongb, B.; Liua, X.; Xuanb, H.; Huangb, Y.; Lina, D. *Analytica Chimica Acta* **2008**, *624*, 269–277.
(27) Lin, J-H, Tseng, W-L. *Reviews in Analytical Chemistry* **2012**, *31*, 153–162.
(28) Brenner, W.; Färber, G.; Herget, T.; Wiesner, C.; Hengstler, J.G.; Thüroff, J.W. *Anticancer Res*. **2003**, *23(5A),* 4001-6.
(29) Chuize, K.; Yuyan, Z.; Zhe, Z.; Tao, L.; Meng, Y.; Qi, Y. *Urology* **2010**, *76(2),* 514.e1-5.
(30) Griner, E.M.; Kazanietz, M.G. *Nat Rev Cancer*. **2007**, *7(4),* 281-94.
(31) Volpe, A.; Finelli, A.; Gill, I.S.; Jewett, M.A.; Martignoni, G.; Polascik, T.J.; Remzi, M.; Uzzo, R.G. *Eur Urol*. **2012**, *62*, 491-504.
(32) Breda, A.; Stepanian, S.V.; Liao, J.; Lam, J.S.; Guazzoni, G.; Stifelman, M.; Perry, K.; Celia, A.; Breda, G.; Fornara, P.; Jackman, S.; Rosales, A.; Palou, J.; Grasso, M.; Pansadoro, V.; Disanto, V.; Porpiglia, F.; Milani, C.; Abbou, C.; Gaston, R.; Janetschek, G.; Soomro, N.A.; de la Rosette, J.; Laguna, M.P.; Schulam, P.G. *J Urol* **2007**, *178*, 47–50.
(33) Duvdevani, M.; Laufer, M.; Kastin, A.; Mor, Y.; Nadu, A.; Hanani, J.; Nativ, O.; Ramon, J. *J Urol* **2005**, *173*, 385–7.
(34) Eberlin, L.S.; Tibshirani, R.J.; Zhang, J.; Longacre, T.A.; Berry, G.J.; Bingham, D.B.; Norton, J.A.; Zare, R.N.; and Poultsides, G.A. *PNAS* **2014**, *111*, 2436-2441.

For TOC Only